Intrinsically disordered nuclear pore proteins show ideal-polymer morphologies and dynamics

Luke K. Davis,[1,2,3] Ian J. Ford,[1,2] Anđela Šarić,[2,3,*] and Bart W. Hoogenboom[1,2,3,†]

[1]*London Centre for Nanotechnology, University College London, London WC1H OAH, United Kingdom*

[2]*Department of Physics and Astronomy, University College London, London WC1E 6BT, United Kingdom*

[3]*Institute for the Physics of Living Systems, University College London, London WC1E 6BT, United Kingdom*

(Dated: June 16, 2019)

Abstract

In the nuclear pore complex (NPC), intrinsically disordered nuclear pore proteins (FG nups) form a selective barrier for transport into and out of the cell nucleus, in a way that remains poorly understood. The collective FG nup behaviour has long been conceptualized either as a polymer brush, dominated by entropic and excluded-volume (repulsive) interactions, or as a hydrogel, dominated by cohesive (attractive) interactions between FG nups. Here we compare mesoscale computational simulations with a wide range of experimental data to demonstrate that FG nups are at the crossover point between these two regimes. Specifically, we find that repulsive and attractive interactions are balanced, resulting in morphologies and dynamics that are close to those of ideal polymer chains. We demonstrate that this property of FG nups yields sufficient cohesion to seal the transport barrier, and yet maintains fast dynamics at the molecular scale, permitting the rapid polymer rearrangements needed for transport events.

INTRODUCTION

Nuclear pore complexes (NPCs) penetrate the nuclear envelope in eukaryotic cells, controlling macromolecular transport between the nucleus and cytoplasm. The NPC enables small ($\lesssim$ 5 nm in size) molecules to cross the nuclear envelope, but hinders the transport of larger macromolecules [1–3]. Larger macromolecular cargoes, however, can diffuse through the NPC if they are bound to nuclear transport receptors that have an affinity to the transport barrier. Remarkably, the NPC maintains the transport barrier while thousands of cargoes shuttle in and out of the cell nucleus per second [4]. This transport barrier consists of proteins (nucleoporins) that are rich in phenylalanine (F) and glycine (G) repeats (hence called FG nups, for FG nucleoporins) and that are grafted to the inner wall of the NPC transport channel. These hydrophobic domains grant the FG nups cohesive properties, which may be counterbalanced by electrostatic interactions [5, 6]. FG nups are intrinsically disordered proteins [7], causing them to behave as flexible polymers [8].

For a long time, there have been conflicting views on the dominant interactions pervading FG nup assemblies, and these views continue to define the interpretation of experimental data. On one hand, repulsive interactions have been postulated to result in entropic polymer-brush behaviour of FG nups [9–11]. On the other hand, cohesive (*i.e.,* attractive) interactions can cause FG nups to form hydrogels *in vitro* [4, 12, 13]. The combined effects of repulsion,

cohesion, grafting, and nanopore confinement lead to a rich landscape of possible polymer behaviour [14–17].

Recently, more nuanced views regarding FG nup interactions have emerged, substantiated by computational models of FG nups at different levels of coarse graining. By defining FG nups down to their amino acid composition, such models can relate, e.g., FG nup behaviour to their chemical composition and explore the effects of mutations [18–20], with the important caveat that the results critically depend on a large number of parameter settings. Complementarily, at a coarser ("mesoscale") level, FG nups have been modelled as homogeneous polymers where the electrostatic, hydrophobic, and hydrophilic interactions are incorporated into one essential interaction parameter [21, 22]. Remarkably, these coarser models have reproduced key functional properties of FG nups, with and without nuclear transport receptors, as observed in experiment [21, 22]. This strongly suggests that NPC transport functionality may be generically understood in terms of mesoscale polymer physics. These and other studies have also indicated that FG nup assemblies display aspects of both entropic and cohesive physical behaviour [16, 21, 22]. Furthermore, there is experimental evidence that isolated intrinsically disordered proteins, including FG nups, show properties that are close to those of "ideal" polymers [23, 24], characterized by a radius of gyration scaling of $R_G \propto N^{1/2}$, N being the number of monomers, where repulsive and attractive interactions balance such that the polymer behaves as if no excluded-volume or other larger-range intramolecular interactions are present [25].

In this letter, we show how such ideal-polymer behaviour compares with experimental data on 27 purified FG domains that are either isolated or grafted at physiological densities (FG nup assemblies) [5, 10, 22, 26, 27]. Specifically, we assess how the experimental morphologies compare with computational predictions on polymer behaviour from assemblies containing repulsive, cohesive, and ideal polymers. Importantly we also investigate how these behaviours translate into the static and dynamic properties of polymers in a context that is relevant to NPC transport functionality.

RESULTS

We model FG nups as freely jointed polymers consisting of N identical beads where one bead, with a diameter and bond length of 0.76 nm, represents two amino acids (Figure 1a).

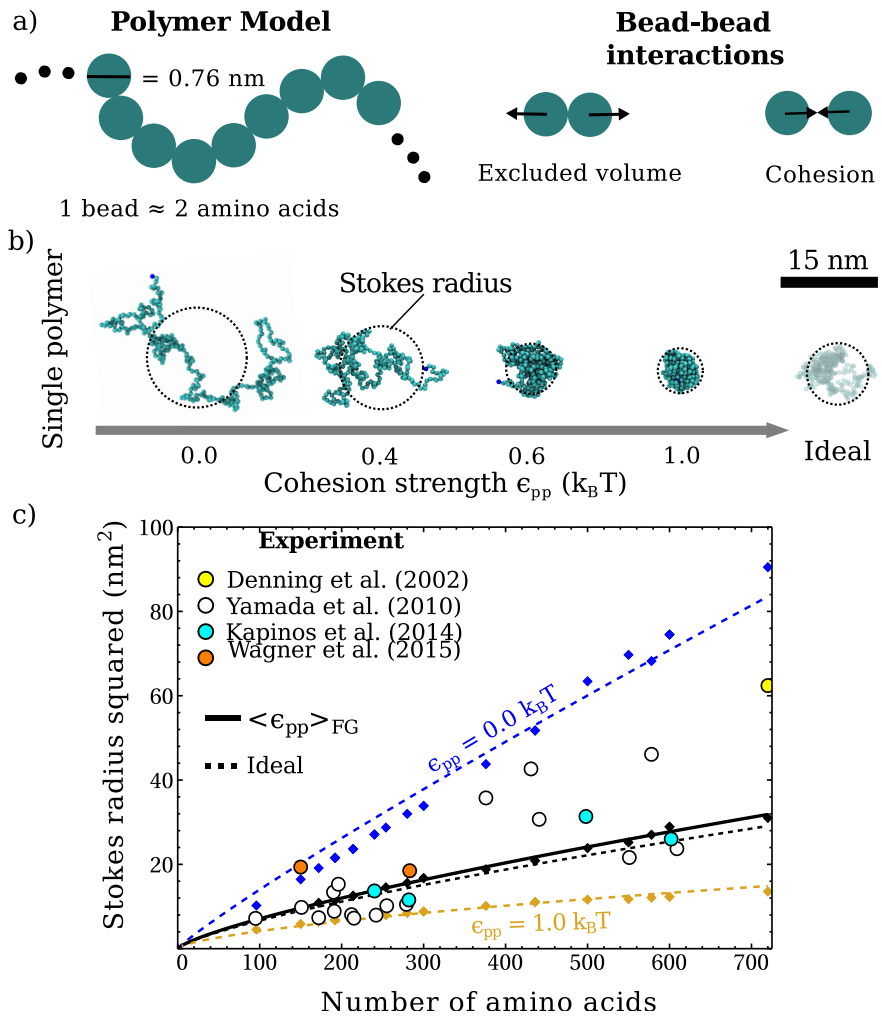

FIG. 1. Parametrization of the polymer model by comparison with experimental Stokes radii [5, 10, 26, 27]. **a)** Illustration of the polymer model (MD). **b)** MD snapshots of a polymer (N = 300 beads) as a function of ϵ_{pp}, alongside an ideal polymer. **c)** Experimental Stokes radii (circles) plotted against FG nup sequence lengths (see Table S1), compared with MD data (diamonds) alongside power law fits of the simulation data (solid and dashed lines).

This choice in polymer model yields a predicted persistence length (0.38 nm) that agrees with experimental data on FG nups and other disordered polypeptide chains [28, 29], and that approaches the excluded-volume of an FG nup (i.e., the sum of the van der Waals volumes of its amino acids, overestimating it by $\sim$ 20% on average, see Table S1). FG nup excluded-volume (repulsive) and cohesive interactions are modelled through a short-ranged pair potential with a minimum value of ϵ_{pp}, which is a measure of the cohesion strength between polymer beads (Figure S1a). Thus defined, ϵ_{pp} is a phenomenological

parameter capturing the general cohesive properties of FG nups. We consider weak attractive interactions, with a $K_D \sim 0.1$ M between two beads, as here found for $0.0\ k_BT \leq \epsilon_{pp} \leq 1.0\ k_BT$ (see Figure S1b and Supplemental Material).

The physiologically relevant ϵ_{pp} was determined by calculating hydrodynamic (Stokes) radii of specific FG constructs using MD simulations, and by comparing these with experimental data [5, 10, 26, 27], using an approach similarly applied elsewhere [30] (see Table S1 for results). Qualitatively, at $\epsilon_{pp} = 0.0\ k_BT$ (no cohesion) a polymer is in a swollen state; for $0.0 < \epsilon_{pp} < 1.0\ k_BT$ polymers adopt morphologies that become increasingly compact with increasing ϵ_{pp}; and at $\epsilon_{pp} = 1.0\ k_BT$ ("high cohesion") a polymer forms a tight ball-like morphology (Figure 1b and Video S1). When all bead-bead interactions are nullified (ideal polymer), the polymer sizes lie – as expected – between the predictions for polymers with no and high cohesion (with excluded-volume).

The average of the parametrized ϵ_{pp} values (see Table S1) yields $\langle \epsilon_{pp} \rangle_{FG} = 0.5 \pm 0.2\ k_BT$ (mean $\pm$ standard deviation, see Figure 1c). Remarkably the experimental data points for polymers with cohesion strength $\langle \epsilon_{pp} \rangle_{FG}$ coincide with the data from ideal polymer simulations (Figure 1c). This is a manifestation of polymer behaviour that typically occurs at Θ-point conditions [25]. Comparing the simulations for $\langle \epsilon_{pp} \rangle_{FG}$ with those for ideal polymers, we also find similar scaling exponents for Stokes radii (Table S2) which are slightly less than the scaling exponents for R_G, as is known for finite length polymers [32].

Importantly, we observe that the match between the mean FG nup behaviour, with $\langle \epsilon_{pp} \rangle_{FG}$, and ideal polymer behaviour is robust against the choice of model. Using a model (with a bead size of 0.57 nm) with lower estimates of the protein volume and persistence length of FG nups, we find a smaller $\langle \epsilon_{pp} \rangle_{FG} = 0.26 \pm 0.06\ k_BT$, yet for this $\langle \epsilon_{pp} \rangle_{FG}$ we still observe an excellent match with the ideal polymer prediction (Figure S2). Generally, to match the experimental data, the FG nup swelling due to excluded-volume interactions (Figure 1b) needs to be counteracted by intramolecular cohesion. As a consequence, overestimates of protein volume, and hence of excluded-volume, lead to larger ϵ_{pp} values in our comparisons with the experimental data. We note that FG nup domains with higher charged/polar content appear more extended [5], which in our analysis translates into smaller ϵ_{pp} values. Interestingly, this further extension can be entirely explained by the larger excluded volume of these specific domains, *i.e.*, without needing to take into account explicit electrostatic interactions (Figure S3).

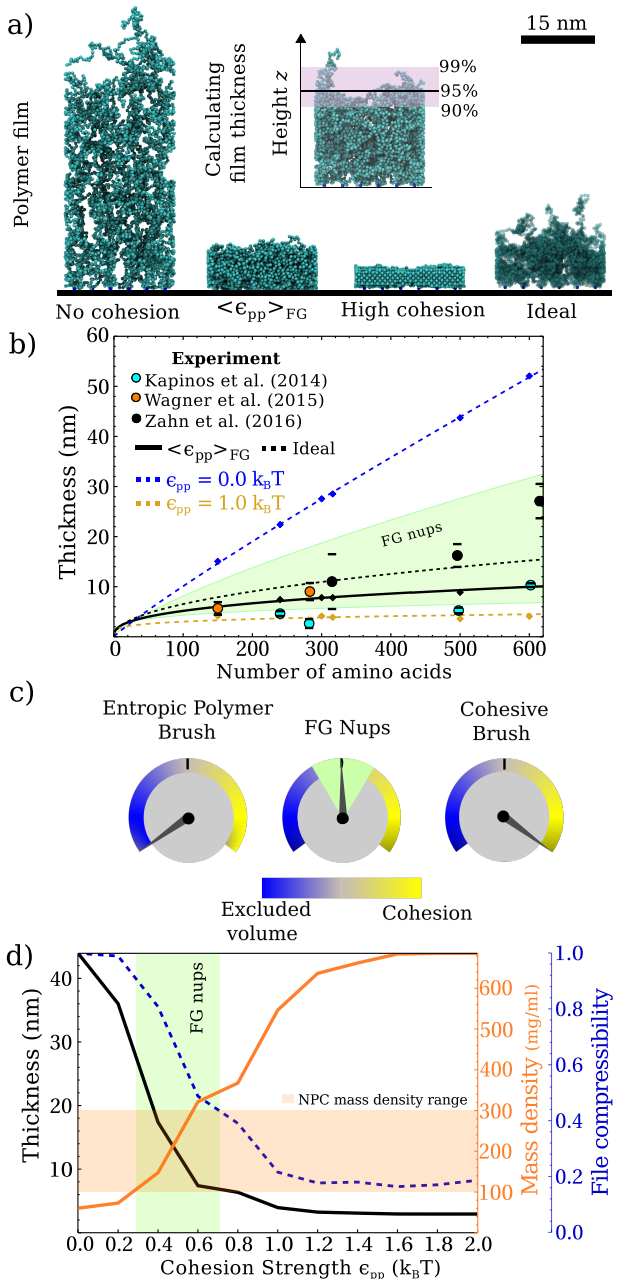

FIG. 2. Comparing the parameterized polymer model with planar assemblies of FG nups. **a)** MD snapshots of polymers ($N = 300$ beads) grafted onto a surface (at a density of 3.2 polymers/100 nm^2) for various interaction regimes. **b)** Experimental film thicknesses (circles) plotted against FG nup sequence lengths. MD simulation data (diamonds) are shown for $\epsilon_{pp} = \{0.0, \langle\epsilon_{pp}\rangle_{FG}, 1.0\}\ k_BT$ alongside ideal polymer data. **c)** An illustration of the balance between excluded-volume and cohesive interactions for FG nups. **d)** Measures of compaction as a function of ϵ_{pp} (MD, see main text). The mass density range, from a simulated NPC, is shown in orange shading [31].

We also tested against experimental data on FG nups that are grafted, at physiological densities, onto a planar surface (polymer film) [10, 22, 27]. MD simulations (Figure 2a and Video S2) for $\langle \epsilon_{pp} \rangle_{FG} = 0.5 \pm 0.2\ k_B T$ yield FG nup film thicknesses (Figure 2b, green shading) that are in agreement with the experimental data (Figure S4), with the exception of three data points (see Supplemental Material for an explanation). With these three exceptions, experimental and computational data for $\langle \epsilon_{pp} \rangle_{FG}$ again show close agreement with the predictions for ideal polymers.

This finding is corroborated by density functional theory (DFT) modelling, in which grafted FG nups are described as ideal polymers interacting with a mean field that is optimized to best represent the net effect of excluded-volume, cohesion, and grafting of the FG nups to a surface (see Supplemental Material) [15]. This DFT yields film thicknesses that are in good agreement with the MD simulations of the same system (Figure S5), and allows us to quantify the effect of molecular interactions via the mean field per polymer in the film (Figure S6). Here the ideal polymer behaviour, where excluded-volume and cohesion balance out (Figure 2c), is articulated via the zero-crossings of the mean field energy per polymer and of the second virial coefficient in the relevant range of ϵ_{pp} (Figure S7).

Next we explore how the identified ideal polymer behaviour translates into functionally relevant properties. Firstly in the ϵ_{pp} range relevant for FG nups, we find that the computed film thickness (Figure 2d) shows a steep change from a swollen polymer film to a compact film. This is confirmed by other measures of film compaction, such as the mass density and file compressibility [33]. The latter quantity corresponding to the losslessly compressed size (in Bytes) of a file containing the MD bead coordinates divided by the losslessly compressed size for $\epsilon_{pp} = 0.0\ k_B T$ (see Supplemental Material). The mass density of the FG nups, in the relevant ϵ_{pp} range, is consistent with the FG nup mass density in the NPC, as estimated using models including finer molecular detail [31].

Interestingly, the change in compaction is even more abrupt (in the relevant ϵ_{pp} range) for FG nups that are assembled in a pore geometry, as here probed by MD simulations on NPC-mimetics based on well-defined numbers and types of FG nups grafted in a DNA origami pore scaffold [34] (Figures 3 and S8, and Video S3). Hence in the physiologically relevant parameter range as determined above, we observe that FG nup assemblies in a nanopore can undergo major conformational changes for only minor changes in intermolecular interactions [15, 35].

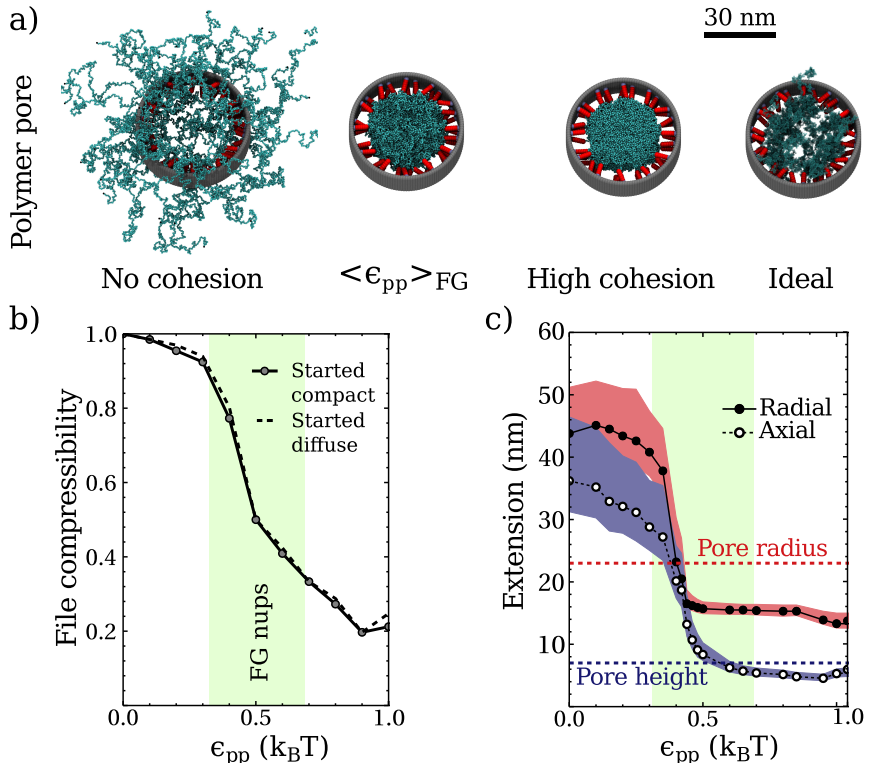

FIG. 3. Investigating polymer morphology in an NPC-mimicking geometry [34]. **a)** MD snapshots of polymers in a pore (polymers in blue; inner pore scaffold in grey; grafting handles in red) for various interaction regimes (48 polymers, $N = 300$ beads). **b)** File compressibility plotted as a function of ϵ_{pp}. **c)** Polymer extension in the pore as a function of ϵ_{pp}. The red (radial) and purple (axial) bands denote the extension thresholds that contain 99% and 90% of the total beads.

Thus far, we have observed that FG nup morphologies on average resemble those of ideal polymers, that they are at the transition between two (extreme) regimes of polymer behaviour, and that at this transition, it is possible to have large conformational changes for small changes in molecular interactions. This latter observation appears to be of significant physiological relevance, as it provides a mechanism by which FG nup assemblies in the NPC may open and close [15] to facilitate transport of large cargoes at millisecond time scales without compromising the transport barrier.

We next investigated the resealing dynamics of the barrier, *i.e.*, how fast and by how much polymers fill the center of the pore following the creation of holes (void of polymers) of 10, 20, and 30 nm diameter in an NPC-mimetic pore system containing 48 polymers [34] (Figures 4a and S9, and Video S4).

We observe that FG nup resealing of the pore can be characterized by two regimes depending on the cohesion strength ϵ_{pp} (Figure 4b,c). For $\epsilon_{pp} \gtrapprox 0.4\ k_BT$, the centre of the pore reaches a maximum polymer density that is approximately double that for $\epsilon_{pp} < 0.4\ k_BT$. We also observe that for $\epsilon_{pp} \gtrapprox 0.4\ k_BT$, the resealing rate appears slower than for $\epsilon_{pp} < 0.4\ k_BT$, where polymers rapidly extend away from their tethering points (Figure S9). We probed the resealing time, τ, which is the time taken for the central density to reach $\approx$ 63 % its equlibrium value (Figure 4c). Notably, for polymers at $\langle \epsilon_{pp} \rangle_{FG}$, the resealing time for "large cargoes" (exceeding 10 nm diameter [1–3]) is similar to that of ideal polymers, albeit that the central density remains at a relatively lower level for the ideal polymer case. This implies that the similarity to ideal polymers also extends to the dynamic behaviour of FG nups. Typically, the resealing times are on the microsecond time-scale, much faster – as needed to inhibit unspecific transport – than the millisecond time scale for transport events, and in agreement with previous simulations [36]. We also observe a sharp transition in resealing time occurring at $0.3\ k_BT < \epsilon_{pp} < 0.4\ k_BT$, which falls in the relevant ϵ_{pp} range.

Finally, we investigate how the cohesive interactions between FG nups affect dynamics at molecular and submolecular length scales. Nuclear magnetic resonance spectroscopy indicates fast (on the picosecond - nanosecond time scale) FG nup residue dynamics [37, 38], presumably indicative of entropically dominated FG nup behaviour. We simulated isolated polymers and measured the durations of bead-bead contacts, *i.e.*, the elapsed time during which the centres of adjacent beads (excluding nearest bonded neighbours) are within the range of the attractive pair potential, (Figure 4d). Of note, the relevant time scales appear rather independent of ϵ_{pp}. The strong dependence of the *collective* FG nup morphology on ϵ_{pp} (Figures 1, 2), is due to the rapid accumulation of many weak *individual* bead-bead contacts upon a moderate increase of ϵ_{pp}, which can be attributed to the higher local bead concentration for larger ϵ_{pp}. Overall, individual FG nups exhibit fast dynamics (picosecond time-scale) at (sub-)molecular length scales, characteristic of their entropic nature. At larger length scales FG nup assemblies, dominated by the collective FG nup molecular interactions, exhibit microsecond dynamics with enhanced resealing (due to cohesion) which is of sufficient speed to maintain the transport barrier.

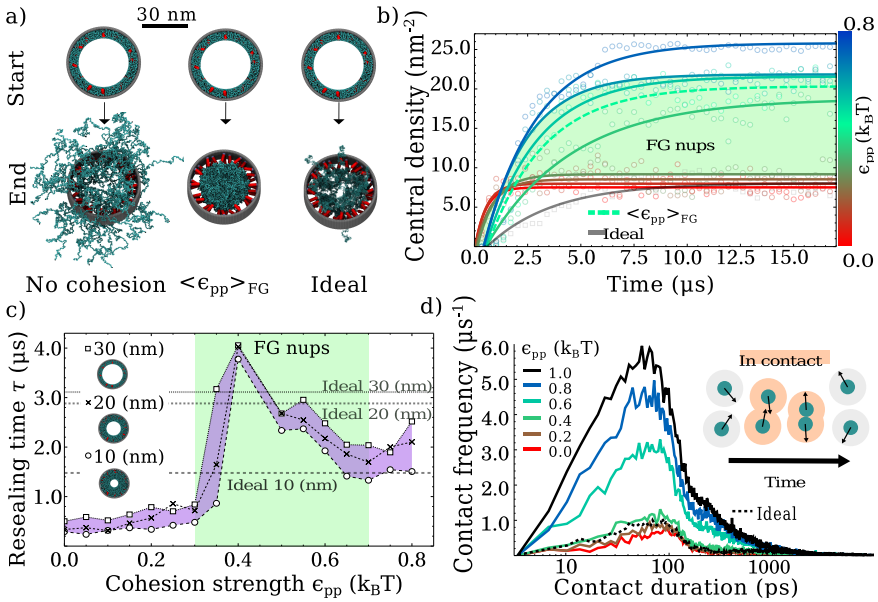

FIG. 4. FG nup dynamics on the mesoscale and molecular scale. **a)** *In silico* polymer resealing in a nanopore [34]. The arrow represents 34 μs (or 10^7 timesteps) of simulation time, pointing to resulting MD snapshots. **b)** The number of beads in a central circular cross-sectional area (5 nm radius) as a function of time. The cohesion strength colour bar represents the range $\epsilon_{pp} = 0.0 - 0.8\ k_BT$ (with 0.1 k_BT increments). Lines represent fits using $\rho(t) = \rho_{max}(1 - \exp(-t/\tau))$, where ρ_{max} is the maximum central density and τ is the resealing time. **c)** τ as a function of ϵ_{pp} alongside resealing times for ideal polymers (dashed). **d)** Distribution of contact durations for a single isolated polymer ($N = 300$ beads).

CONCLUSION

In summary, we find that FG nup morphologies do not agree with predictions for purely entropic behaviour, dominated by (repulsive) excluded-volume interactions, nor with predictions for gel-like, strongly condensed behaviour governed by (attractive) cohesive interactions. This is fully consistent with previous studies [16, 21, 22, 24]. More surprisingly, we find that, on average, FG nup morphologies are consistent with the predictions for polymers that are characterized by the balance of repulsive and cohesive molecular interactions, *i.e.*, the FG nups on average behave like ideal polymers, at or close to their Θ-point in physiological buffer solutions. FG nup mesoscale dynamics (microseconds) are also in agreement with predictions for ideal polymers, and are such that FG nup assemblies can reseal fast

enough to reseal the barrier after transport events, which occur on millisecond time scales. Additionally, the rapid movement of FG nups on the molecular scale — maintained through a large range of cohesion strengths — will facilitate the uptake and release of nuclear transport factors and associated cargoes [39], whereas the accumulation of many weakly cohesive interactions facilitates the tight sealing of the NPC transport barrier. Taken together, this physical picture reconciles previous – apparently contradictory – identifications of FG nup assemblies as "entropic brushes" or "gels", and provides a conceptual framework with which to interpret the transport selectivity of the NPC.

We thank Dino Osmanović (MIT), Roy Beck (Tel-Aviv), Larissa Kapinos (Basel), Roderick Lim (Basel), Ralf Richter (Leeds), and Anton Zilman (Toronto) for discussions. This work was funded by the Royal Society (A.Š.) and the UK Engineering and Physical Sciences Research Council (EP/L504889/1, B.W.H.).

* a.saric@ucl.ac.uk

† b.hoogenboom@ucl.ac.uk

[1] T. Jovanovic-Talisman and A. Zilman, Protein Transport by the Nuclear Pore Complex: Simple Biophysics of a Complex Biomachine, Biophys. J. **113**, 6 (2017).

[2] I. V. Aramburu and E. A. Lemke, Floppy but not sloppy: Interaction mechanism of FG-nucleoporins and nuclear transport receptors, Semin. Cell Dev. Biol. **68**, 34 (2017).

[3] G. J. Stanley, A. Fassati, and B. W. Hoogenboom, Biomechanics of the transport barrier in the nuclear pore complex, Semin. Cell Dev. Biol. **68**, 42 (2017).

[4] B. B. Hülsmann, A. A. Labokha, and D. Görlich, The permeability of reconstituted nuclear pores provides direct evidence for the selective phase model, Cell **150**, 738 (2012).

[5] J. Yamada, J. L. Phillips, S. Patel, G. Goldfien, A. Calestagne-Morelli, H. Huang, R. Reza, J. Acheson, V. V. Krishnan, S. Newsam, A. Gopinathan, E. Y. Lau, M. E. Colvin, V. N. Uversky, and M. F. Rexach, A Bimodal Distribution of Two Distinct Categories of Intrinsically Disordered Structures with Separate Functions in FG Nucleoporins, Mol. Cell. Proteomics **9**, 2205 (2010).

[6] M. Peyro, M. Soheilypour, B. Lee, and M. Mofrad, Evolutionarily Conserved Sequence Features Regulate the Formation of the FG Network at the Center of the Nuclear Pore Complex, Sci.

Rep. **5**, 15795 (2015).

[7] D. P. Denning, S. S. Patel, V. Uversky, A. L. Fink, and M. Rexach, Disorder in the nuclear pore complex: The FG repeat regions of nucleoporins are natively unfolded, Proc. Natl. Acad. Sci. **100**, 2450 (2003).

[8] R. Y. Lim, B. Fahrenkrog, J. Köser, K. Schwarz-Herion, J. Deng, and U. Aebi, Nanomechanical basis of selective gating by the nuclear pore complex, Science. **318**, 640 (2007).

[9] R. L. Schoch, L. E. Kapinos, and R. Y. H. Lim, Nuclear transport receptor binding avidity triggers a self-healing collapse transition in FG-nucleoporin molecular brushes, Proc. Natl. Acad. Sci. **109**, 16911 (2012).

[10] L. E. Kapinos, R. L. Schoch, R. S. Wagner, K. D. Schleicher, and R. Y. H. Lim, Karyopherin-centric control of nuclear pores based on molecular occupancy and kinetic analysis of multivalent binding with FG nucleoporins, Biophys. J. **106**, 1751 (2014).

[11] B. L. Timney, B. Raveh, R. Mironska, J. M. Trivedi, S. J. Kim, D. Russel, S. R. Wente, A. Sali, and M. P. Rout, Simple rules for passive diffusion through the nuclear pore complex, J. Cell Biol. **215**, 57 (2016).

[12] A. A. Labokha, S. Gradmann, S. Frey, B. B. Hülsmann, H. Urlaub, M. Baldus, and D. Görlich, Systematic analysis of barrier-forming FG hydrogels from Xenopus nuclear pore complexes, EMBO J. **32**, 204 (2013).

[13] H. B. Schmidt and D. Görlich, Nup98 FG domains from diverse species spontaneously phase-separate into particles with nuclear pore-like permselectivity, Elife **4**, e04251 (2015).

[14] O. Peleg, M. Tagliazucchi, M. Kröger, Y. Rabin, and I. Szleifer, Morphology control of hairy nanopores, ACS Nano **5**, 4737 (2011).

[15] D. Osmanovic, J. Bailey, A. H. Harker, A. Fassati, B. W. Hoogenboom, and I. J. Ford, Bistable collective behavior of polymers tethered in a nanopore, Phys. Rev. E - Stat. Nonlinear, Soft Matter Phys. **85**, 1 (2012), arXiv:1109.0419.

[16] N. B. Eisele, A. A. Labokha, S. Frey, D. Görlich, and R. P. Richter, Cohesiveness tunes assembly and morphology of FG nucleoporin domain meshworks - Implications for nuclear pore permeability, Biophys. J. **105**, 1860 (2013).

[17] D. Osmanovic and Y. Rabin, Effect of Grafting on Aggregation of Intrinsically Disordered Proteins, Biophys. J. **114**, 534 (2018), arXiv:1706.03337.

[18] M. Tagliazucchi, O. Peleg, M. Kröger, Y. Rabin, and I. Szleifer, Effect of charge, hydrophobicity, and sequence of nucleoporins on the translocation of model particles through the nuclear pore complex, Proc. Natl. Acad. Sci. **110**, 3363 (2013).

[19] R. Gamini, W. Han, J. E. Stone, and K. Schulten, Assembly of Nsp1 Nucleoporins Provides Insight into Nuclear Pore Complex Gating, PLoS Comput. Biol. **10**, e1003488 (2014).

[20] A. Ghavami, E. Van der Giessen, and P. R. Onck, Sol–gel transition in solutions of FG-Nups of the nuclear pore complex, Extrem. Mech. Lett. **22**, 36 (2018).

[21] A. Vovk, C. Gu, M. G. Opferman, L. E. Kapinos, R. Y. H. Lim, R. D. Coalson, D. Jasnow, and A. Zilman, Simple biophysics underpins collective conformations of the intrinsically disordered proteins of the Nuclear Pore Complex, Elife **5**, e10785 (2016).

[22] R. Zahn, S. Ehret, C. A. Callis, D. Osmanovic, S. Frey, M. Stewart, C. You, D. Gorlich, R. P. Richter, and B. W. Hoogenboom, A physical model describing the interaction of nuclear transport receptors with FG nucleoporin domain assemblies, Elife **5**, e14119 (2016).

[23] H. Hofmann, A. Soranno, A. Borgia, K. Gast, D. Nettels, and B. Schuler, Polymer scaling laws of unfolded and intrinsically disordered proteins quantified with single-molecule spectroscopy, Proc. Natl. Acad. Sci. **109**, 16155 (2012).

[24] G. Fuertes, N. Banterle, K. M. Ruff, A. Chowdhury, D. Mercadante, C. Koehler, M. Kachala, G. Estrada Girona, S. Milles, A. Mishra, P. R. Onck, F. Gräter, S. Esteban-Martín, R. V. Pappu, D. I. Svergun, and E. A. Lemke, Decoupling of size and shape fluctuations in heteropolymeric sequences reconciles discrepancies in SAXS vs. FRET measurements, Proc. Natl. Acad. Sci. **114**, E6342 (2017).

[25] P.-G. de. Gennes, *Scaling concepts Polym. Phys.* (Cornell University Press, Ithaca, NY, 1979).

[26] D. P. Denning, V. Uversky, S. S. Patel, A. L. Fink, and M. Rexach, The Saccharomyces cerevisiae nucleoporin Nup2p is a natively unfolded protein, J. Biol. Chem. **277**, 33447 (2002).

[27] R. S. Wagner, L. E. Kapinos, N. J. Marshall, M. Stewart, and R. Y. H. Lim, Promiscuous binding of karyopherinβ1 modulates FG nucleoporin barrier function and expedites NTF2 transport kinetics, Biophys. J. **108**, 918 (2015).

[28] R. Y. H. Lim, N.-P. Huang, J. Koser, J. Deng, K. H. A. Lau, K. Schwarz-Herion, B. Fahrenkrog, and U. Aebi, Flexible phenylalanine-glycine nucleoporins as entropic barriers to nucleocytoplasmic transport, Proc. Natl. Acad. Sci. **103**, 9512 (2006).

[29] G. Stirnemann, D. Giganti, J. M. Fernandez, and B. J. Berne, Elasticity, structure, and relaxation of extended proteins under force, Proc. Natl. Acad. Sci. **110**, 3847 (2013).

[30] A. Ghavami, E. van der Giessen, and P. R. Onck, Coarse-grained potentials for local interactions in unfolded proteins, J. Chem. Theory Comput. **9**, 432 (2012).

[31] A. Ghavami, L. M. Veenhoff, E. Van Der Giessen, and P. R. Onck, Probing the disordered domain of the nuclear pore complex through coarse-grained molecular dynamics simulations, Biophys. J. **107**, 1393 (2014).

[32] A. J. Ladd and D. Frenkel, Computer Simulation Studies of Static and Dynamical Scaling in Dilute Solutions of Excluded-Volume Polymers, Macromolecules **25**, 3435 (1992).

[33] R. Avinery, M. Kornreich, and R. Beck, Universal and efficient entropy estimation using a compression algorithm, arXiv:1709.10164v3. (2018), arXiv:1709.10164.

[34] P. D. E. Fisher, Q. Shen, B. Akpinar, L. k. Davis, K. K. H. Chung, D. Baddeley, A. Saric, T. J. Melia, B. W. Hoogenboom, C. Lin, and C. P. Lusk, A Programmable DNA Origami Platform for Organizing Intrinsically Disordered Nucleoporins within Nanopore Confinement, ACS Nano **12**, 1508 (2018).

[35] S. Ro, A. Gopinathan, and Y. W. Kim, Interactions between a fluctuating polymer barrier and transport factors together with enzyme action are sufficient for selective and rapid transport through the nuclear pore complex, Phys. Rev. E **98**, 1 (2018).

[36] R. Moussavi-Baygi and M. R. Mofrad, Rapid Brownian Motion Primes Ultrafast Reconstruction of Intrinsically Disordered Phe-Gly Repeats Inside the Nuclear Pore Complex, Sci. Rep. **6**, 1 (2016).

[37] L. E. Hough, K. Dutta, S. Sparks, D. B. Temel, A. Kamal, J. Tetenbaum-Novatt, M. P. Rout, and D. Cowburn, The molecular mechanism of nuclear transport revealed by atomic-scale measurements, Elife **4**, e10027 (2015).

[38] S. Milles, D. Mercadante, I. V. Aramburu, M. R. Jensen, N. Banterle, C. Koehler, S. Tyagi, J. Clarke, S. L. Shammas, M. Blackledge, F. Gräter, and E. A. Lemke, Plasticity of an Ultrafast Interaction between Nucleoporins and Nuclear Transport Receptors, Cell **163**, 734 (2015).

[39] R. Hayama, S. Sparks, L. M. Hecht, K. Dutta, J. M. Karp, C. M. Cabana, M. P. Rout, D. Cowburn, and N. M. Allewell, Thermodynamic characterization of the multivalent interactions underlying rapid and selective translocation through the nuclear pore complex, J. Biol. Chem. **293**, 4555 (2018).